# Phase-Controlled Bistability of a Dark Soliton Train in a Polariton Fluid

V. Goblot,[1,*] H. S. Nguyen,[1,†] I. Carusotto,[2] E. Galopin,[1] A. Lemaître,[1] I. Sagnes,[1] A. Amo,[1] and J. Bloch[1,3]
[1]Centre de Nanosciences et de Nanotechnologies, CNRS, Univ. Paris-Sud, Université Paris-Saclay, C2N—Marcoussis, 91460 Marcoussis, France
[2]INO-CNR BEC Center and Dipartimento di Fisica, Università di Trento, I-38123 Povo, Italy
[3]Département de Physique, Ecole Polytechnique, Université Paris Saclay, F-91128 Palaiseau Cedex, France
(Received 8 July 2016; published 16 November 2016)

We use a one-dimensional polariton fluid in a semiconductor microcavity to explore the nonlinear dynamics of counterpropagating interacting Bose fluids. The intrinsically driven-dissipative nature of the polariton fluid allows us to use resonant pumping to impose a phase twist across the fluid. When the polariton-polariton interaction energy becomes comparable to the kinetic energy, linear interference fringes transform into a train of solitons. A novel type of bistable behavior controlled by the phase twist across the fluid is experimentally evidenced.

DOI: 10.1103/PhysRevLett.117.217401

Dark solitons are among the fundamental nonlinear collective excitations of one-dimensional (1D) quantum degenerate fluids with positive mass and repulsive interactions. They are characterized by a dip in a uniform background density and a jump in the macroscopic phase across it. The shape and size of the dip is given by the interplay of mass and nonlinearity. Because of the universality of the mechanisms necessary to their formation, dark solitons have been observed in a wide variety of systems ranging from Bose-Einstein condensates of cold atoms [1–3] and optical fibers [4], to thin magnetic films [5]. Interestingly, dark solitons have also been observed in nonlinear open-dissipative systems, in particular, in semiconductor microcavities [6–9], and are attracting great interest in view of photonic applications [10].

Semiconductor microcavities have recently appeared as an excellent platform to study the nonlinear dynamics of interacting Bose fluids in a photonic context [11]. Their elementary excitations are exciton polaritons, bosonic quasiparticles arising from the strong coupling between quantum well excitons and photons confined in the microcavity. While their excitonic component provides significant repulsive interactions, the fast escape of photons out of the microcavity makes polaritons an intrinsically open-dissipative system, requiring continuous wave pumping to achieve a steady state. A number of quantum fluid effects has been studied in semiconductor microcavities, including superfluidity [12], diffusive Goldstone modes [13], Bogoliubov excitation spectrum [14], solitary bright waves [15,16], and the hydrodynamic nucleation of quantized vortices [17,18] and dark solitons [7,8].

In addition to the possibility of *in situ* and time-resolved imaging of the fluid dynamics, a remarkable feature of driven-dissipative systems is that a resonant drive allows setting the local phase of the wave function [11]. It is then possible to externally manipulate the boundary conditions and impose a controlled phase pattern across a polariton fluid. This was first explored in a two-dimensional polariton condensate in which a spatial vortex phase profile was imposed on the polariton field, resulting in persistent currents with high orbital momentum [19]. This technique opens up a new world for the exploration of the elementary excitations of polariton quantum fluids. In particular, it has been proposed that by imposing a phase twist across the fluid via the external pumping, the superfluid fraction could be measured [20], different Josephson dynamical regimes could be addressed [21,22], and the controlled nucleation of dark solitons could be implemented [23].

In this Letter, we report on the study of counterpropagating interacting polariton fluids resonantly excited in a 1D semiconductor cavity. At high excitation power, polariton-polariton interactions are responsible for the self-organization of a dark soliton train, which is directly evidenced by spatial imaging of the 1D channel. When scanning the excitation power, the abrupt disappearance of solitons reflects the discrete nature of these nonlinear excitations. Interestingly, varying the phase difference between the two pumping beams, we are able to impose a phase twist across the fluid which controls not only the position of the soliton train, but also the parity of their number. A novel type of bistable behavior appears when scanning the phase twist up and down, at constant power.

Our sample, grown by molecular beam epitaxy, consists of a $\lambda$ GaAs cavity surrounded by two $Ga_{0.9}Al_{0.1}As/Ga_{0.05}Al_{0.95}As$ Bragg mirrors with 26 (30) pairs in the top (bottom) mirror. A single 8 nm $In_{0.05}Ga_{0.95}As$ quantum well is inserted at the cavity center. The Rabi splitting resulting from the exciton-photon strong coupling amounts to 3.5 meV. Electron beam lithography and dry etching are used to fabricate photonic wires of 3 $\mu$m width and 200 $\mu$m length [Fig. 1(b)]. The experiments are performed at a temperature of 10 K. The photoluminescence is collected in

 

transmission geometry through the sample back, and real- and momentum-space emission is imaged on a CCD camera coupled to a spectrometer. A polarizer selects the emission polarized along the wire.

First, the polariton dispersion in the wire has been characterized by nonresonant photoluminescence, using a cw single-mode Ti:sapphire laser. Figure 1(a) shows the momentum-space emission, evidencing the lower and upper polariton 1D subbands. We deduce an exciton-photon detuning $\delta = E_C(k=0) - E_X(k=0) \approx -3.5$ meV, where $E_C(k)$ is the bare photon energy and $E_X(k)$ the bare exciton energy. Close to $k = 0$, the lower polariton branch can be approximated by a parabola, $E(k) = E_0 + \hbar^2 k^2/2m$, where $m = 4 \times 10^{-5} m_e$ is the polariton effective mass and $m_e$ the free electron mass.

The focus of this Letter is to investigate the dynamics of a pair of counterflowing polariton fluids. To create them, we use a resonant cw laser split in two separate beams, linearly polarized along the wire and focused at normal incidence onto two 8 $\mu$m diameter spots separated by a distance $d$. The laser energy $\hbar\omega_p$ is blueshifted by $\Delta E = \hbar\omega_p - E_0$ with respect to the lower polariton energy $E_0$ at $k = 0$ [see Fig. 1(a)]. The phase difference $\Delta\varphi$ between the two beams can be varied using a delay stage controlled by a piezoelectric actuator added to the path of one of the excitation beams.

Figure 1(c) shows the polariton emission, spatially resolved along the wire, measured for a low pumping power $P = 8$ mW well in the linear regime. The saturated bright regions correspond to the excitation spots positions, and the bright regions outside the wire, above and below the spots, correspond to laser light scattered by the wire edges, and are thus not relevant. Even though the excitation spots are at normal incidence, their finite angular aperture allows injecting polaritons with wave vectors $k_f = \pm\sqrt{2m\Delta E}/\hbar = \pm 0.53\ \mu\text{m}^{-1}$ [11]. Between the two excitation spots, we observe a regular fringe pattern with a spacing of $s = 6.0\ \mu\text{m} = \pi/k_f$, arising from interference of the two counterpropagating polariton waves (a sinusoidal fit of the fringe pattern is shown in the Supplemental Material [24]). The position of the fringe pattern is determined by the boundary conditions imposed by the excitation spots, namely, the distance between them and their phase difference $\Delta\varphi$. When $\Delta\varphi$ is scanned, we observe a continuous spatial displacement of the interference pattern [see Fig. 1(e)], a behavior characteristic of the linear regime.

Superfluidity and the nucleation of dark solitons are features of quantum fluids showing up when the interparticle interaction energy is comparable to the kinetic energy. In our system, the interaction energy is $\hbar g n$, where $g$ is the polariton-polariton interaction constant and $n$ the polariton density, controlled by the excitation power. When the latter is ramped up into the nonlinear regime, a first threshold is observed when the blueshift due to polariton-polariton interactions under the pump spots equals $\Delta E$, resulting in an abrupt increase of the polariton density [see Fig. 2(d)]. When the power is further ramped up, a second threshold is observed with a change of the spatial

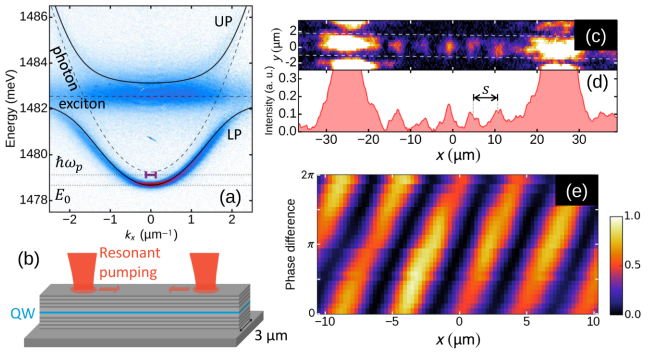


FIG. 1. (a) Far-field photoluminescence measured under nonresonant pumping. (Solid lines) Theoretical fits of the lower and upper polariton branches and (dashed lines) bare exciton and photon energy. The horizontal segment shows the energy and width for the resonant excitation conditions. (b) Sketch of the experimental configuration. (c) Spatially resolved emission measured along the wire in the linear regime, for $P = 8$ mW, $\Delta E = 0.27$ meV, $d = 50$ $\mu$m, and $\Delta\varphi \approx 0$. Dotted lines indicate the wire edges. The color scale is saturated in regions under the spots. (d) Measured intensity profile integrated in the transverse direction. (e) Intensity profile measured along the wire as a function of $\Delta\varphi$ for similar pumping parameters, well in the linear regime.

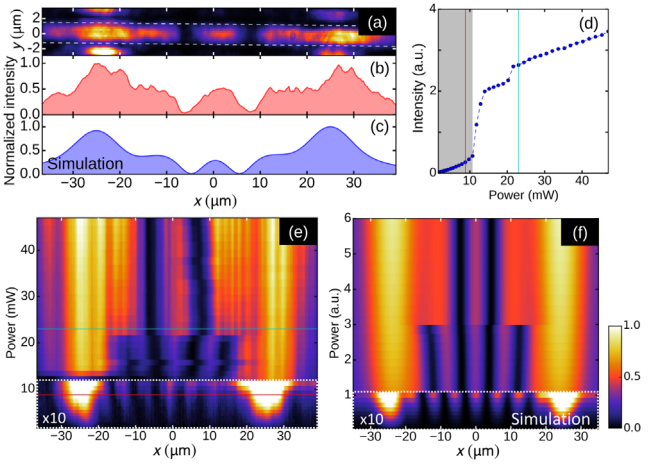


FIG. 2. (a) Spatially resolved emission measured along the wire for $P = 23$ mW ($\Delta E = 0.27$ meV, $d = 50$ $\mu$m, $\Delta\varphi \approx 0$). (b) Intensity profile integrated over the transverse direction. (c) Corresponding calculated emission profile. (d) Total measured emission intensity (integrated along both the transverse and longitudinal directions) as a function of pump power. The shaded gray region corresponds to the linear regime. (e) Measured and (f) calculated emission profile when scanning the power up (the low power data have been amplified by a factor of 10 for clarity). The horizontal red [blue] line corresponds to the profile shown in Fig. 1(d) [2(b)].

pattern. A similar threshold behavior has been reported in a 1D polariton fluid in a configuration in which polaritons are excited by a single beam and reflected by an external potential [27].

A typical emission pattern above the second threshold is shown in Fig. 2(a) for $\Delta\varphi \approx 0$. It strongly differs from the linear case [Fig. 1(c)]: two density dips, dropping almost to zero, are visible in an otherwise almost constant high density profile. Those dips are identified as dark solitons—nonlinear collective excitations of the fluid. They are well fitted by the characteristic hyperbolic tangent function, and the characteristic $\pi$ phase jump of the wave function across the soliton was experimentally confirmed by measuring the interference between the polariton emission and a constant-phase reference beam [24].

Figure 2(e) reveals that the number of solitons depends on the excitation power. Directly above the first threshold at $P_{\mathrm{th}} = 12$ mW, four solitons are present in the region between the spots. Further increasing the excitation power, we observe at $P = 21$ mW the abrupt expulsion of two solitons so that only two of them remain. Interestingly, the polariton density between the spots and outside of the dark solitons is almost independent of the pumping power. Notice that the observed expulsion of two solitons, replaced by regions of high polariton density, is responsible for the small jump in total emitted intensity that is visible at the second threshold [see Fig. 2(d)]. Throughout the whole power scan in Fig. 2(d), the number of solitons remains even because of the symmetry of the excitation conditions. Indeed, since we impose $\Delta\varphi \approx 0$, the polariton wave function must remain symmetric, implying an even number of solitons.

To reproduce these experimental observations, we solve a 1D Gross-Pitaevskii equation that includes pump and loss terms, and consider only the lower polariton branch [28]. The evolution of the polariton wave function $\Psi(x)$ is given by

$$i\hbar\frac{\partial\Psi(x,t)}{\partial t} = \left[E_0 - \frac{\hbar^2}{2m}\frac{\partial^2\Psi(x,t)}{\partial x^2} + \hbar g|\Psi(x,t)|^2\right]\Psi(x,t) - i\frac{\hbar\gamma}{2}\Psi(x,t) + iF(x)e^{-i\omega_p t}, \quad (1)$$

where $\gamma$ is the polariton decay rate. $F(x) = F_0 f(x)$, with $|F_0|^2$ being proportional to the total power of the coherent drive, and $f(x)$ is a complex function describing the spatial profile and the relative phase of the pump beams. The steady-state solutions of the equation are obtained numerically for the experimentally measured linewidth $\hbar\gamma = 47\mu$eV, $E_0 = 1478.57$ meV, $\Delta E = 0.27$ meV and Gaussian spots of width $w = 8\ \mu$m separated by $d = 50\ \mu$m. We take an interaction constant $\hbar g = 0.3\ \mu\mathrm{eV}\,\mu\mathrm{m}$ [29]. Figure 2(f) shows the calculated polariton density $|\Psi(x)|^2$ as a function of the excitation power $|F_0|^2$. The calculations perfectly reproduce the low power interferences and the abrupt transition to the nonlinear regime resulting in the nucleation of four dark solitons and, at higher power, two dark solitons [Fig. 2(c)].

The nucleation of solitons in the nonlinear regime, and the abrupt change in their number when increasing the excitation power can be intuitively understood from the hydrodynamics of the polariton flow. In the steady state, in the central region far from the excitation spots, the real part of Eq. (1) multiplied by $\Psi^*(x)$ can be written as a "local" energy conservation as follows:

$$\hbar\omega_p = E_0 - \frac{\hbar^2}{2m}\frac{\mathrm{Re}(\Psi^*\nabla^2\Psi)(x)}{n(x)} + \hbar g n(x). \quad (2)$$

The imaginary part of the steady state equation gives a continuity equation that accounts for the losses due to the finite polariton lifetime and the injection from the pumping beams. Equation (2) shows that the energy per polariton is fixed by $\omega_p$. Thus, locally, $\hbar\omega_p$ must be equal to the sum of three terms: the single-polariton energy $E_0$ at $k = 0$; a kinetic term $(-(\hbar^2/2m)[\mathrm{Re}(\Psi^*\nabla^2\Psi)/n(x)])$; and a polariton-polariton interaction term $[\hbar g n(x)]$.

The specific dark soliton profile at a given pump power is a result of the local interplay between the kinetic and interaction terms. In the core of a soliton, where the density is low and its second order derivative is high, the kinetic term dominates over interactions, while it is the opposite in the high density regions far from the core. At pump densities just above the first nonlinear threshold, the polariton flow from the pump spots towards the central region contains a high kinetic energy that needs to be accommodated in the form of a large number of solitons, four in the case depicted in Fig. 2(e) in the 12–21 mW range. When the excitation power is further increased, the higher density in the wire results in an increase of interactions. In the balance established by Eq. (2), a higher weight of the interaction term must be accompanied by a decrease of the kinetic term, resulting in the expulsion of solitons. The results of the numerical simulations [Fig. 2(c), (f)] reproduce quantitatively the features observed in the experiment: at low pump intensities, there is just a linear interference whereas when interactions become significant, the sinusoid transforms into a soliton train, more precisely an elliptic function shape [24], as first discussed in Refs. [30] and [31].

We now address bistability in the wire, a well-established behavior displayed by nonlinear dissipative systems as a function of driving intensity [11,32,33]. Usually this effect is observed in a configuration where the polariton field is frozen in a single mode. When, as in the present situation, multimode polariton fluids are considered, the complex spatial dynamics is expected to give rise to conceptually different bistability or even multistability effects [34–36]. As a first example, we notice that the abrupt change in soliton number occurs at different excitation powers when

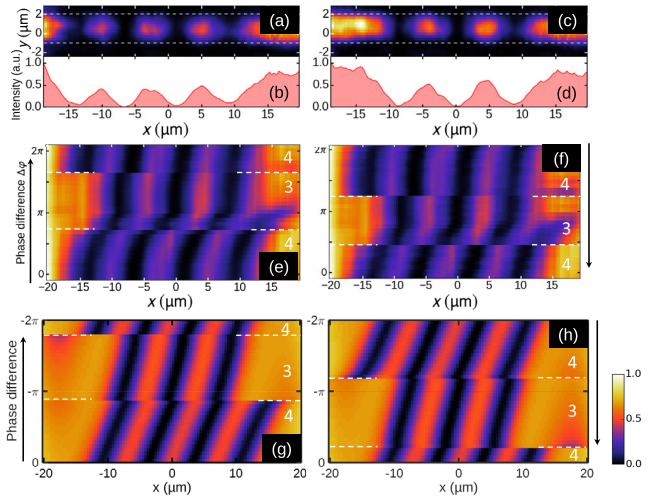


FIG. 3. (a),(c) Spatially resolved emission for $P = 57$ mW, $\Delta E = 0.37$ meV, $d = 50$ $\mu$m and (a) $\Delta\varphi \approx 0$; (c) $\Delta\varphi \approx \pi$. (b),(d) Corresponding intensity profiles integrated over the transverse direction. (e),(f) Measured and (g),(h) calculated intensity profiles for increasing (e),(g) and decreasing (f),(h) phase difference $\Delta\varphi$ between the spots. White dotted lines indicate the value of $\Delta\varphi$ for which a soliton is expelled or generated. The measured number of solitons is indicated in white.

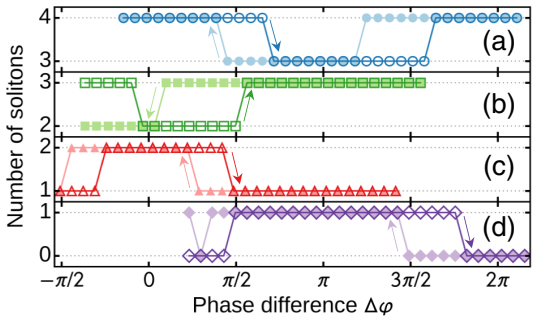


FIG. 4. (a)–(d) Number of solitons measured when scanning $\Delta\varphi$ up (open symbols) and down (closed symbols). (a) Same parameters as in Figs. 3(e) and 3(f); (b) $\Delta E = 0.21$ meV, $P = 42$ mW, $d = 60$ $\mu$m; (c) $\Delta E = 0.35$ meV, $P = 90$ mW, $d = 40$ $\mu$m; (d) $\Delta E = 0.20$ meV, $P = 103$ mW, $d = 40$ $\mu$m. The fluctuations due to phase noise in the experimental setup are estimated on the order of $\pm 0.03\pi$.

the power is scanned downward than when it is ramped up [24]: two different soliton patterns can thus be observed for the same excitation power.

An even more intriguing bistable behavior occurs when the excitation power is kept constant while scanning the phase twist $\Delta\varphi$ across the polariton fluid imposed by the excitation lasers. Figure 3(a)–3(d) shows the polariton density profiles for a fixed excitation power and different values of $\Delta\varphi$. For $\Delta\varphi = 0$ [Fig. 3(a)] a symmetric profile is observed with four solitons. On the contrary, when $\Delta\varphi = \pi$ [Fig. 3(c)], an antisymmetric profile is measured, with only three solitons, consistent with the antisymmetric boundary conditions. The transition between the two situations takes place abruptly when scanning $\Delta\varphi$, as shown in Fig. 3(e) (white dashed lines), attesting to the nonlinear character of the fluid [in contrast to the smooth rigid motion of fringes in the linear regime that is visible in Fig. 1(e)]. This transition can be understood in a similar way to the case of Fig. 2, where a scan in power induces a change in interaction energy. In the present situation, the phase twist results in a change in kinetic energy across the fluid, which is accommodated via the expulsion or addition of a soliton to the fluid pattern. When approaching $\Delta\varphi = \pi$, the choice between the expulsion and the inclusion of a soliton is settled by the most stable solution at the considered excitation power.

Remarkably, when scanning $\Delta\varphi$ in the upward and downward directions for a fixed excitation power we observe a bistable behavior, as predicted in Ref. [23]. In Fig. 3(f), $\Delta\varphi$ is now decreased, starting from the situation $\Delta\varphi = 2\pi$ from Fig. 3(e). The expulsion or generation of single solitons takes place at different values of $\Delta\varphi$ than in the upward scan. In other words, there exist values of the phase difference between the beams, for which two different profiles—with either four or three solitons—are stable: we evidence a bistability entirely controlled by the relative phase of the pumping beams.

The numerical simulations presented in Figs 3(g) and 3(h) are in good qualitative agreement with the measured phase scan, including the bistable behavior. There are, however, some differences: the theoretical patterns shown in the two panels transform into each other under the $\Delta\varphi \to 2\pi - \Delta\varphi$ transformation, while in the experiment, this symmetry is only approximately satisfied. Indeed, the simulation shows a more regular displacement of the soliton pattern than the measurement. For instance, when three solitons are stable, the measured pattern appears almost fixed in space for a wide range of $\Delta\varphi$. This can be explained by the presence of disorder in the wire, as confirmed by simulations when introducing a small potential dip to model a defect [24]. The slightly smaller bistability range observed in the experiments as compared to simulations could also be caused by disorder [24], as well as by phase noise in the pump beams.

Figure 4 summarizes the measured number of solitons versus $\Delta\varphi$ in the upward and downward scans for different configurations of excitation powers and distances $d$. Abrupt switching between trains with $N$ and $N+1$ solitons is observed for $N$ ranging from 0 to 3. In each of these situations, we observe a well-defined phase-controlled bistability.

In conclusion, we have demonstrated the ability to generate and control soliton trains in a 1D polariton quantum fluid. The ability to impose a controllable phase twist across the fluid using a coherent drive allows us to reveal a novel bistable behavior. This experimental configuration offers a new perspective to explore the excitation spectrum of soliton trains in pump and probe experiments.

Moreover, exploiting the polarization degree of freedom of polaritons, formation of spin domains [23], and half soliton trains [37–39] have been predicted. Finally, from a more general perspective, as the response of a quantum fluid to a phase perturbation is quantitatively related to its superfluid fraction [20,40,41], our experiment opens the way to the experimental measurement of this quantity, crucial in the theory of driven dissipative quantum fluids [42].

This work was supported by the French National Research Agency (ANR) program Labex NanoSaclay projects Qeage (ANR- 11-IDEX-0003-02) and ICQOQS (ANR-10-LABX-0035), the French RENATECH network, the ERC Grant Honeypol and the EU-FET Proactive Grant AQUS (Project No. 640800). I. C. is grateful to F. Dalfovo for insightful discussions.

*valentin.goblot@lpn.cnrs.fr
†Present address: Institut de Nanotechnologies de Lyon, Ecole Centrale de Lyon, CNRS (UMR5270), 69134 Ecully, France.

[1] S. Burger, K. Bongs, S. Dettmer, W. Ertmer, K. Sengstock, A. Sanpera, G. V. Shlyapnikov, and M. Lewenstein, Phys. Rev. Lett. **83**, 5198 (1999).
[2] J. Denschlag *et al.*, Science **287**, 97 (2000).
[3] P. Engels and C. Atherton, Phys. Rev. Lett. **99**, 160405 (2007).
[4] A. M. Weiner, J. P. Heritage, R. J. Hawkins, R. N. Thurston, E. M. Kirschner, D. E. Leaird, and W. J. Tomlinson, Phys. Rev. Lett. **61**, 2445 (1988).
[5] M. Chen, M. A. Tsankov, J. M. Nash, and C. E. Patton, Phys. Rev. Lett. **70**, 1707 (1993).
[6] Y. Larionova, W. Stolz, and C. O. Weiss, Opt. Lett. **33**, 321 (2008).
[7] A. Amo *et al.*, Science **332**, 1167 (2011).
[8] G. Grosso, G. Nardin, F. Morier-Genoud, Y. Léger, and B. Deveaud-Plédran, Phys. Rev. Lett. **107**, 245301 (2011).
[9] R. Hivet *et al.*, Nat. Phys. **8**, 724 (2012).
[10] T. Ackemann, W. Firth, and G.-L. Oppo, Adv. At. Mol. Opt. Phys. **57**, 323 (2009).
[11] I. Carusotto and C. Ciuti, Rev. Mod. Phys. **85**, 299 (2013).
[12] A. Amo, J. Lefrère, S. Pigeon, C. Adrados, C. Ciuti, I. Carusotto, R. Houdré, E. Giacobino, and A. Bramati, Nat. Phys. **5**, 805 (2009).
[13] D. Ballarini, D. Sanvitto, A. Amo, L. Viña, M. Wouters, I. Carusotto, A. Lemaitre, and J. Bloch, Phys. Rev. Lett. **102**, 056402 (2009).
[14] V. Kohnle, Y. Léger, M. Wouters, M. Richard, M. T. Portella-Oberli, and B. Deveaud-Plédran, Phys. Rev. Lett. **106**, 255302 (2011).
[15] A. Amo *et al.*, Nature (London) **457**, 291 (2009).
[16] M. Sich, D. N. Krizhanovskii, M. S. Skolnick, A. V. Gorbach, R. Hartley, D. V. Skryabin, E. A. Cerda-Mendez, K. Biermann, R. Hey, and P. V. Santos, Nat. Photonics **6**, 50 (2012).
[17] G. Nardin, G. Grosso, Y. Leger, B. Pietka, F. Morier-Genoud, and B. Deveaud-Pledran, Nat. Phys. **7**, 635 (2011).
[18] D. Sanvitto *et al.*, Nat. Photonics **5**, 610 (2011).
[19] D. Sanvitto *et al.*, Nat. Phys. **6**, 527 (2010).
[20] A. Janot, T. Hyart, P. R. Eastham, and B. Rosenow, Phys. Rev. Lett. **111**, 230403 (2013).
[21] D. Sarchi, I. Carusotto, M. Wouters, and V. Savona, Phys. Rev. B **77**, 125324 (2008).
[22] I. A. Shelykh, D. D. Solnyshkov, G. Pavlovic, and G. Malpuech, Phys. Rev. B **78**, 041302 (2008).
[23] M. Y. Petrov and A. V. Kavokin, Phys. Rev. B **88**, 035308 (2013).
[24] See Supplemental Material at http://link.aps.org/supplemental/10.1103/PhysRevLett.117.217401 for additional experimental data and numerical simulations, which includes Refs. [25,26].
[25] V. V. Konotop and L. Pitaevskii, Phys. Rev. Lett. **93**, 240403 (2004).
[26] D. J. Frantzeskakis, G. Theocharis, F. K. Diakonos, P. Schmelcher, and Y. S. Kivshar, Phys. Rev. A **66**, 053608 (2002).
[27] H. S. Nguyen, D. Gerace, I. Carusotto, D. Sanvitto, E. Galopin, A. Lemaître, I. Sagnes, J. Bloch, and A. Amo, Phys. Rev. Lett. **114**, 036402 (2015).
[28] I. Carusotto and C. Ciuti, Phys. Rev. Lett. **93**, 166401 (2004).
[29] L. Ferrier, E. Wertz, R. Johne, D. D. Solnyshkov, P. Senellart, I. Sagnes, A. Lemaître, G. Malpuech, and J. Bloch, Phys. Rev. Lett. **106**, 126401 (2011).
[30] J. H. Marburger and F. S. Felber, Phys. Rev. A **17**, 335 (1978).
[31] L. D. Carr, C. W. Clark, and W. P. Reinhardt, Phys. Rev. A **62**, 063610 (2000).
[32] R. W. Boyd, *Nonlinear Optics* (Academic, New York, 2008).
[33] A. Baas, J. P. Karr, H. Eleuch, and E. Giacobino, Phys. Rev. A **69**, 023809 (2004).
[34] T. K. Paraïso, M. Wouters, Y. Leger, F. Mourier-Genoud, and B. Deveaud-Pledran, Nat. Mater. **9**, 655 (2010).
[35] S. R. K. Rodriguez, A. Amo, I. Sagnes, L. L. Gratiet, E. Galopin, A. Lemaitre, and J. Bloch, Nat. Commun. **7**, 11887 (2016).
[36] C. Ouellet-Plamondon, G. Sallen, F. Morier-Genoud, D. Y. Oberli, M. T. Portella-Oberli, and B. Deveaud, Phys. Rev. B **93**, 085313 (2016).
[37] F. Pinsker and H. Flayac, Phys. Rev. Lett. **112**, 140405 (2014).
[38] H. Terças, D. D. Solnyshkov, and G. Malpuech, Phys. Rev. Lett. **110**, 035303 (2013).
[39] H. Terças, D. D. Solnyshkov, and G. Malpuech, Phys. Rev. Lett. **113**, 036403 (2014).
[40] L. Pitaevskii and S. Strindgari, *Bose-Einstein Condensation* (Oxford University Press, Oxford, 2003).
[41] I. Carusotto and Y. Castin, Phys. Rev. A **84**, 053637 (2011).
[42] G. Wachtel, L. M. Sieberer, S. Diehl, and E. Altman, Phys. Rev. B **94**, 104520 (2016).